Loss of astrocyte cholesterol synthesis disrupts neuronal function and alters whole-body metabolism

Heather A. Ferris[a], Rachel J. Perry[b], Gabriela V. Moreira[b], Gerald I. Shulman[b,c,d], Jay D. Horton[e], and C. Ronald Kahn[a,1]

[a]Joslin Diabetes Center, Harvard Medical School, Boston, MA 02215; [b]Department of Internal Medicine, Yale University, New Haven, CT 06520; [c]Cellular & Molecular Physiology, Yale University, New Haven, CT 06520; [d]Howard Hughes Medical Institute, Yale University, New Haven, CT 06520; and [e]Department of Molecular Genetics, University of Texas Southwestern, Dallas, TX 75390

Contributed by C. Ronald Kahn, December 22, 2016 (sent for review August 23, 2016; reviewed by Robert H. Eckel and Simon Fisher)

Cholesterol is important for normal brain function. The brain synthesizes its own cholesterol, presumably in astrocytes. We have previously shown that diabetes results in decreased brain cholesterol synthesis by a reduction in sterol regulatory element-binding protein 2 (SREBP2)-regulated transcription. Here we show that coculture of control astrocytes with neurons enhances neurite outgrowth, and this is reduced with SREBP2 knockdown astrocytes. In vivo, mice with knockout of SREBP2 in astrocytes have impaired brain development and behavioral and motor defects. These mice also have altered energy balance, altered body composition, and a shift in metabolism toward carbohydrate oxidation driven by increased glucose oxidation by the brain. Thus, SREBP2-mediated cholesterol synthesis in astrocytes plays an important role in brain and neuronal development and function, and altered brain cholesterol synthesis may contribute to the interaction between metabolic diseases, such as diabetes and altered brain function.

brain cholesterol metabolism | glial cells | SREBP2 | metabolic regulation | glucose oxidation

The brain is one of the most cholesterol-rich organs in the body, with cholesterol playing an important role in membrane fluidity, vesicle formation, and synaptogenesis (1). Cholesterol levels are tightly controlled by sterol regulatory element-binding protein 2 (SREBP2), the major transcription factor regulating cholesterol synthetic genes (2). In contrast to fatty acids, which are in equilibrium with the rest of the body, nearly all brain cholesterol is synthesized in the brain because cholesterol-carrying lipoproteins, with the exception of some very dense HDL, cannot readily cross the blood–brain barrier (3–5).

When cholesterol is abundant, SREBP2 precursor remains sequestered in the endoplasmic reticulum by SREBP cleavage activating protein (SCAP). As cholesterol is needed, SCAP shuttles SREBP2 to the Golgi for cleavage into a transcriptionally active form that translocates to the nucleus, binds to sterol regulatory elements in DNA, and activates transcription of enzymes of cholesterol synthesis (2). Insulin can regulate SREBP2 expression and activity, in part via two insulin-induced regulatory proteins, Insig1 and Insig2 (6, 7). Furthermore, in insulin-deficient diabetes, there is a decrease in SREBP2 and SCAP in the brain leading to decreased brain cholesterol synthesis (8). We have previously shown that both neurons and glial cells express SREBP2 and the enzymes of cholesterol synthesis, and in both cell types expression of the cholesterol synthesis pathway is stimulated by insulin (7).

Among the subtypes of glia, astrocytes serve the most diverse roles, providing both structural support to neurons and playing a major role in maintaining the blood–brain barrier. In addition, astrocytes provide a variety of metabolic functions, including storage of glycogen and uptake of ions and neurotransmitters from the synaptic cleft (9, 10).

Astrocytes/glial cells have also been suggested to play an important role in brain cholesterol metabolism. When neuronal-like retinal ganglion cells are grown in culture and exposed to glia-conditioned media, there is increased synapse formation (11). Cholesterol is a key mediator of this effect, suggesting that glial cells synthesize and transport cholesterol to neurons via lipoprotein particles. This finding may help explain the strong genetic link between the ε4 isoform of the cholesterol carrier ApoE and Alzheimer disease (AD). Indeed, deletion of LRP1, the major receptor for ApoE on neurons, results in impaired dendritic spine development and neurodegeneration with aging (12). Overactivity of this pathway may also produce adverse effects. Hyperlipidemia in humans has been associated with AD, and whole-body overexpression of SREBP2, which results in loading of cholesterol in brain, worsens pathology in a mouse model of AD (13, 14).

In the present study, we have defined the effects of SREBP2 and cholesterol synthesis in astrocytes using two astrocyte-specific SREBP2 knockout (KO) models. We find that loss of astrocyte-SREBP2 in vitro results in impaired dendrite outgrowth from neurons in coculture. In vivo, loss of SREBP2 in astrocytes alters brain development, resulting in abnormal social, memory, and motor behaviors, as well as multiple metabolic defects, including reduction in adiposity and an altered balance of carbohydrate and lipid oxidation, both at the whole-body level and in the brain.

Results

SREBP2 in Astrocytes Is Required for Normal Neurite Outgrowth. As a first step to determine if SREBP2-mediated astrocyte cholesterol synthesis has an effect on neurons, we cultured GT1-7 mouse hypothalamic cells with C6 rat glioma cells in transwell plates that allow the cells to share nutrients through the media without making physical contact. The glioma cells were stably transfected with lentivirus containing either a scrambled siRNA (shScramble) or siRNA against *Srebf2* (shSrebf2), the gene that encodes SREBP2. Knockdown of *Srebf2* decreased both the total and cleaved forms of SREBP2 protein by ∼60% (Fig. S1*A*) and

Significance

Cholesterol is important for normal brain function and it is believed that astrocytes produce most brain cholesterol. We have previously shown that diabetes results in decreased brain cholesterol synthesis by a reduction in the transcription factor sterol regulatory element-binding protein 2 (SREBP2). Using a mouse model in which SREBP2 has been knocked out in astrocytes, we show that astrocyte SREBP2 is required for normal brain development and behavior. Furthermore, this results in a shift in metabolism driven by increased brain glucose oxidation. Thus, SREBP2-mediated cholesterol synthesis in astrocytes plays an important role in brain development and function, and altered brain cholesterol synthesis may contribute to the interaction between diabetes and altered brain function.

Author contributions: H.A.F. and C.R.K. designed research; H.A.F., R.J.P., and G.V.M. performed research; G.I.S. and J.D.H. contributed new reagents/analytic tools; H.A.F., R.J.P., and C.R.K. analyzed data; and H.A.F., R.J.P., G.I.S., and C.R.K. wrote the paper.

Reviewers: R.H.E., University of Colorado School of Medicine; and S.F., University of Utah School of Medicine.

The authors declare no conflict of interest.

[1]To whom correspondence should be addressed. Email: c.ronald.kahn@joslin.harvard.edu.

This article contains supporting information online at www.pnas.org/lookup/suppl/doi:10.1073/pnas.1620506114/-/DCSupplemental.

PHYSIOLOGY

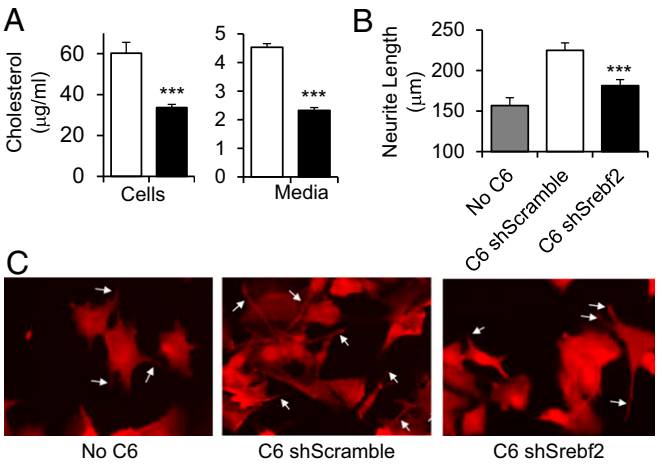

Fig. 1. Loss of SREBP2 from glia inhibits neurite outgrowth. SREBP2 was knocked down in C6 rat glioma cells by stable transfection with a lentiviral delivered shRNA against *Srebf2* or a control shScramble. (*A*) Cholesterol content of cells and cholesterol secreted into serum-free media were measured using the Amplex red assay. $n = 3$ per group. (*B* and *C*) The GT1-7 hypothalamic mouse cell line was grown alone or in coculture using transwells with C6 shScramble or C6 shSrebf2, and neurite length was measured using ImageJ ($n = 146$, 244 and 246 neurites measured, respectively). Student's *t* test ***$P < 0.001$ compared with C6 shScramble. White arrows indicate examples of neurites. (Magnification: 10×.)

caused an ∼50% reduction in cholesterol content in the C6 glioma cells, as well as in cholesterol secreted into the media (Fig. 1*A*). Although there was some decrease in full-length SREBP1, the active cleaved form of SREBP1 was unchanged (Fig. S1*B*), and there was no change in free-fatty acid content in the cells (Fig. S1*C*). Triglyceride levels were barely detectable, consistent with previous reports (15). When GT1-7 cells were grown in transwells with control C6 shScramble cells above them, there was a 46% increase in average neurite length compared with GT1-7 cells grown alone (Fig. 1 *B* and *C*), indicating that glial cells produce a factor that enhances neurite growth. In contrast, when GT1-7 cells were cocultured with *Srebf2*-knockdown glioma cells, there was only a 15% increase in neurite length, consistent with the important factor being cholesterol.

SREBP2 Expression in Astrocytes Is Required for Normal Brain Development. To determine the role of astrocyte cholesterol synthesis in vivo, we created an astrocyte-specific conditional knockout of SREBP2 by breeding mice expressing hGFAP-cre with mice in which the *Srebf2* gene contained lox sites on either side of exon 1. Glial fibrillary acidic protein (*GFAP*) is highly expressed in astrocytes and hGFAP-cre induces recombination beginning at embryonic day (E) 14.5 (16). Homozygous SREBP2 KO pups (hGFAP-cre;$Srebf2^{lox/lox}$, designated G-SB2KO) were born at normal Mendelian ratios and, in contrast to mice with KO of SCAP from astrocytes or whole brain (8, 17), were healthy and viable for the length of the study (10 mo). Gross examination and dissection revealed microcephaly with a 28% reduction in brain weight (3-mo-old males, 343 ± 11 mg vs. 478 ± 5 mg in controls, $P < 0.001$) (Fig. 2 *A* and *B*), with no change in markers of specific cell types (Fig. S2*A*). Serial sections through the brain showed that volume loss was most dramatic in the cortex, hippocampus, and white-matter tracks, such as the corpus callosum (Fig. 2*C*), and in the motor cortex and hippocampus there was a >50% reduction in *Srebf2* transcript levels (Fig. 2*D*), indicating the high efficacy of gene recombination in these areas. This result was accompanied by a trend toward increased activation of astrocytes as measured by *Gfap* expression in these areas (Fig. S2*B*). The cortex also showed a small decrease in expression of PSD95, a postsynaptic marker (Fig. S2*C*). In contrast, the amygdala and hypothalamus, which are comparatively poor in astrocytes, did not have clear reductions in mass and showed no decrease in *Srebf2* mRNA or synaptic markers (Fig. 2*D* and Fig. S2*C*). There was also no evidence of recombination in the liver, the other major site of *Srebf2* expression (Fig. S2*D*).

Histological sections through the corpus callosum, an astrocyte-rich area, revealed plentiful immunofluorescence staining for GFAP in both control and G-SB2KO mice (Fig. 2*E*, *Upper*). In the control mice, staining for SREBP2 showed the highest levels of colocalization with GFAP-stained astrocytes. In G-SB2KO mice there was a decrease in SREBP2 staining in astrocytes, but a large increase in neurons, suggesting that neurons were compensating for the loss of cholesterol synthesis by astrocytes. Even in the thalamus, where GFAP staining of astrocytes was low, there was a massive increase in SREBP2 in the G-SB2KO compared with controls (Fig. 2*E*, *Lower*). Total cholesterol content per milligram of tissue was decreased 10–15% in the hypothalamus and cortex, and to a

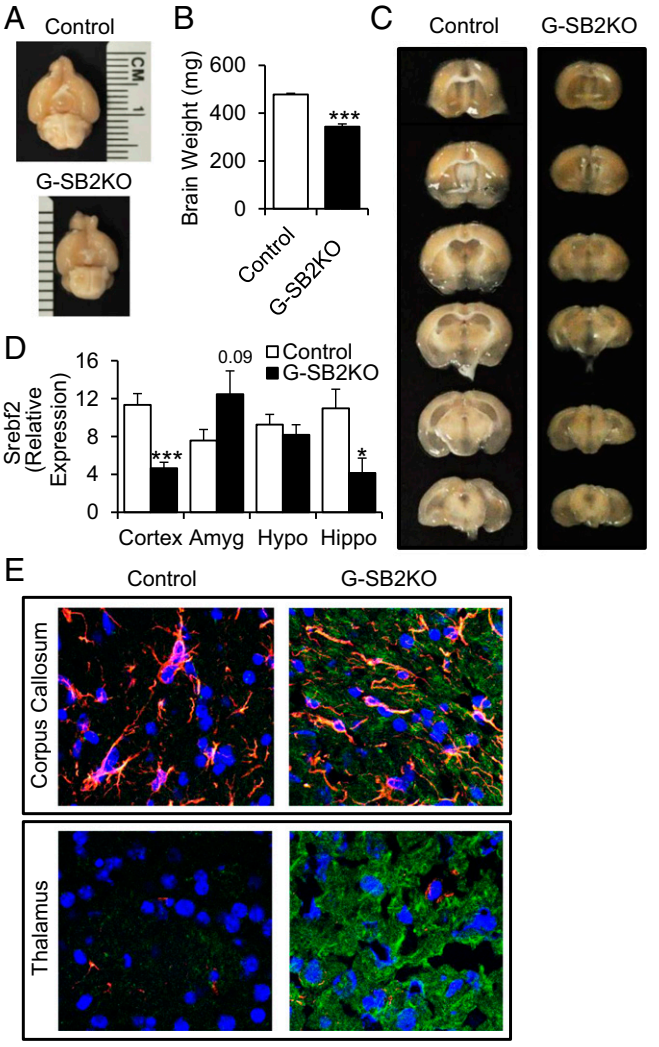

Fig. 2. Homozygous KO of SREBP2 from astrocytes impairs brain development. hGFAP-cre;$Srebf2^{lox/lox}$ mice (designated throughout as G-SB2KO) were compared with littermate controls. (*A* and *B*) Brains of G-SB2KO mice weighed less than controls. $n = 6$ per group. (*C*) Consecutive 1-mm slices through fresh brain. (*D*) Expression of *Srebf2* measured by quantitative PCR (qPCR) from dissected brain regions, cortex, amygdala (Amyg), hypothalamus (Hypo), and hippocampus (Hippo). $n = 5$ control, 4 G-SB2KO. (*E*) Immunostaining for GFAP (red), SREBP2 (green), DAPI (blue), and colocalization (yellow) in corpus callosum and thalamus. Representative 40× confocal images of $n = 3$ control, 2 G-SB2KO. Student's *t* test *$P < 0.05$, ***$P < 0.001$ compared with control.

lesser extent in other regions of the brain (Fig. S2*E*). Serum cholesterol and triglycerides were unaffected (Table S1). These data suggest that in G-SB2KO mice there is a loss in SREBP2/cholesterol synthesis in astrocytes, which is partially compensated for by an increase in cholesterol production by neurons leading to an overall decrease in brain mass with abnormal development, particularly in areas with high astrocyte content.

Loss of Astrocyte SREBP2 Is Associated with Behavioral Abnormalities. Brain function was assessed using a battery of behavioral tests. Social behavior was assessed by measuring nest-building ability. In this test, individually housed mice were given eight strips of paper towel, and the next day the quality of the paper nest created by the mouse was scored on a scale of 1–4, with 4 being best (Fig. 3*A*) (18). As shown in Fig. 3*B*, G-SB2KO mice showed a significant impairment in nest-building quality ($P < 0.05$).

Learning and memory were assessed using a Stone T-maze (19). Mice were placed in the maze that was submerged in 2 cm of water to encourage the mice to complete the maze. Although all of the control mice were able to be trained, one-third of KO mice could not be trained to complete the maze ($P < 0.05$) (Fig. 3*C*). Of the mice able to complete the maze, the number of wrong turns for each run of the maze was counted as the mice ran the maze a total of seven times over 2 d. Both groups improved with each training run, with the control mice trending toward better performance than the KOs over the course of the experiment (Fig. S3*A*). More importantly, when retested 1 wk after the learning trials, the G-SB2KO mice made significantly more mistakes than the controls, indicating a defect in memory retention (10.2 ± 1.1 vs. 6.2 ± 0.8 wrong turns for controls, $P < 0.01$) (Fig. 3*D*). A similar trend was seen 1 mo after the original learning trials (13.0 ± 1.8 vs. 8.1 ± 1.6 wrong turns for controls, $P = 0.06$). Because rotating the maze 180° increased significantly the number of wrong turns made by the control mice from 4.2 ± 1.0–11.2 ± 2.9 ($P < 0.05$), it was clear that the mice used spatial cues to navigate the maze, implying that this is primarily a test of hippocampal memory.

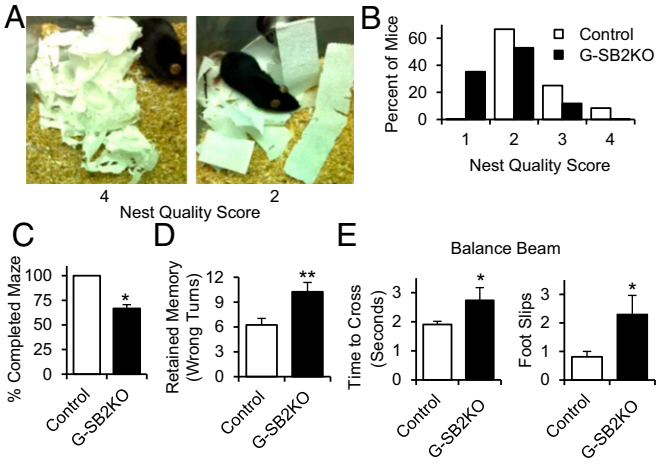

Fig. 3. G-SB2KO mice have multiple neurologic defects. (*A*) Examples of nests, scored on a scale from 1 to 4, showing a nest scoring 4 (*Left*) and 2 (*Right*). (*B*) Distribution of nesting scores, $n = 12$ control, 17 G-SB2KO, $P < 0.05$ by Wilcoxon Rank Sum. Eleven control and 12 G-SB2KO mice were trained in a Stone T-maze. (*C*) Four of the 12 G-SB2KO mice could not be trained to complete the maze. All 11 controls were trainable. $P < 0.05$ by two-proportion test. (*D*) One week after completing maze training, mice were retested and the average of three runs is shown. $n = 11$ control, 8 G-SB2KO. Mice were trained to cross a 12-mm-wide balance beam, then recorded crossing the balance beam two times and the average (*E*) time to cross and number of foot slips were reported. $n = 8$ control, 5 G-SB2KO, 9-wk-old females. Student's *t* test $^*P < 0.05$, $^{**}P < 0.01$.

Motor coordination—that is, the time to cross a 12-mm by 50-cm balance beam—was also significantly increased (2.7 ± 0.4 vs. 1.9 ± 0.1 s, $P < 0.05$), and KO mice had significantly more foot slips than the controls (2.3 ± 0.7 vs. 0.8 ± 0.2 foot slips, $P < 0.05$) (Fig. 3*E*). This result was true for both genders (Fig. S3*B*) and at multiple ages (Fig. S3*C*). The impairment in G-SB2KO mice was not because of muscle weakness, as there was no difference between groups in grip strength (Fig. S3*D*). Taken together, these data demonstrate the requirement for intact SREBP2 in astrocytes for normal social behavior, memory, and coordinated movement.

G-SB2KO Mice Have Altered Body Composition. As early as 5 wk of age, male G-SB2KO mice showed lower body weights compared with control littermates (20.0 ± 0.7 vs. 23.7 ± 0.4 g, $P = 0.001$). The weight difference was also present in females and increased with time, such that by 4 mo of age, female G-SB2KO mice weighed 20% less than controls (19.6 ± 0.7 vs. 24.1 ± 1.1 g, $P < 0.01$) (Fig. S4*A*). Dual-energy X-ray absorptiometry (DXA) demonstrated that the difference in weight in the G-SB2KO mice was because of a reduction in both lean mass (16.1 ± 0.6 vs. 19 ± 0.5 g, $P < 0.01$) and fat mass (2.7 ± 0.2 vs. 4.4 ± 0.9 g, $P = 0.09$), although the latter did not reach significance (Fig. S4*A*). Femur length was the same between groups, demonstrating that the mice were not dwarfed (1.36 ± 0.02 vs. 1.35 ± 0.02 cm for controls, $P = 0.53$).

G-SB2KO mice were also protected from weight gain associated with aging. Between 3 and 9 mo of age, male control mice gained 10.4 ± 0.9 g of weight, whereas G-SB2KO mice only gained 4.3 ± 1.3 g (Fig. S4*B*) ($P < 0.01$). At 9 mo of age, DXA assessment of the male mice demonstrated a significant 25% reduction in lean mass (22.2 ± 1.0 vs. 29.9 ± 1.3 g in controls, $P < 0.001$) and an impressive 72% reduction in fat mass (3.9 ± 0.8 vs. 14.1 ± 1.2 g, $P < 0.001$) (Fig. S4*C*). This result was again associated with no difference in femur length (1.32 ± 0.04 vs. 1.38 ± 0.02 cm in controls, $P = 0.19$). Necropsy revealed differences in all fat depots, with a 79% decrease in visceral fat pad weight (0.36 ± 0.09 vs. 1.68 ± 0.54 g, $P < 0.05$) (Fig. 4*A*), a 66% decrease in subcutaneous (SQ) fat pad weight (0.30 ± 0.06 vs. 0.87 ± 0.18 g, $P = 0.01$), and a 48% reduction in interscapular brown fat weight (0.45 ± 0.02 vs. 0.86 ± 0.20 g, $P = 0.07$). Histological examination revealed that this result was because of smaller size of adipocytes in the white and brown fat pads of G-SB2KO mice. This occurred without any evidence of fat accumulation in the liver (Fig. 4*B*). Indeed, G-SB2KO mice had significantly lower liver weight than controls (0.79 ± 0.04 vs. 1.07 ± 0.08 g, $P = 0.01$) (Fig. 4*A*), as well as a trend toward decreased muscle weight.

Increased activation of the sympathetic nervous system can result in weight loss. However, there were no differences is blood pressure or pulse rate between the groups and no differences in urine metanephrine or normetanephrines (Table S1). Activation of the sympathetic nervous system also controls thermogenesis from brown fat, which can result in energy expenditure (20). However, when mice were challenged with 4 °C cold exposure for 24 h to activate brown fat, G-SB2KO mice were able to maintain body temperature similar to controls (Fig. S5*A*). Expression of mRNA for markers of brown fat activation, such as uncoupling protein 1 (*Ucp1*), PR domain zinc finger protein 16 (*Prdm16*), cell death-inducing DFFA-like effector A (*Cidea*), and deiodinase iodothyronine type II (*Dio2*) were also similar in the interscapular brown fat pads of G-SB2KO and control mice (Fig. S5*B*), and in both controls and G-SB2KO mice *Ucp1* expression in brown fat showed a clear induction with cold challenge (Fig. S5*C*). In addition, SQ and visceral fat depots from mice housed at room temperature showed no difference in mRNA expression for *Ucp1*, *Prdm16*, or *Cidea* between control and G-SB2KO mice (Table S2). Thus, the smaller fat pads in G-SB2KO mice could not be attributed to brown fat activation or browning of the white fat pads. Serum hormones frequently associated with weight change, including triiodothyronine (T3), thyroxine (T4), leptin, corticosterone, and fasting insulin, and insulin tolerance testing were also equivalent between control and G-SB2KO mice (Fig. S6*A* and Table S1).

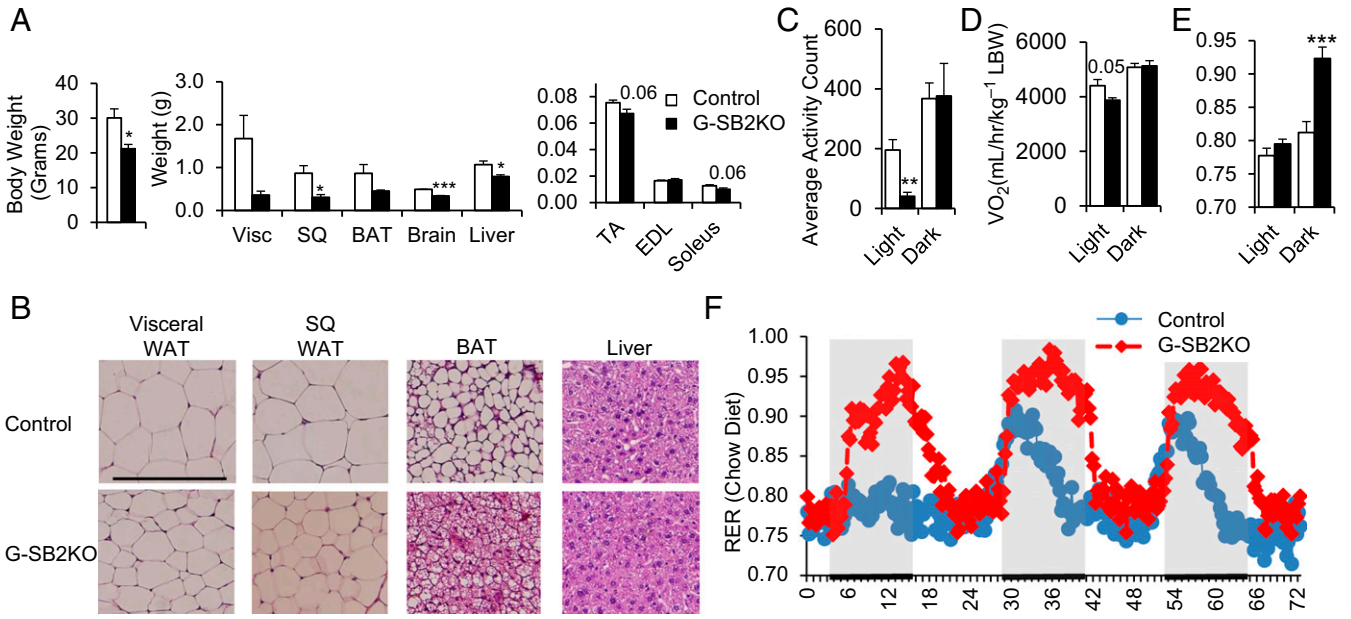

Fig. 4. G-SB2KO mice have altered body composition and metabolism. (*A*) Ten-month-old females were dissected and tissue weights reported. $n = 6$ per group. (*B*) H&E staining of fat pads and livers from 3- to 4-mo-old males. (Scale bar, 200 μm.) BAT, brown adipose tissue; EDL, extensor digitorum longus; TA, tibialis anterior; WAT, white adipose tissue. Four-month-old female mice on chow diet were placed in metabolic cages for 72 h and (*C*) activity counts (beam breaks per 15-min interval, averaged over the light or dark cycle), (*D*) VO_2, and (*E* and *F*) RER were determined. $n = 6$ per group. Student's *t* test $^*P < 0.05$, $^{**}P < 0.01$, $^{***}P < 0.001$.

The enteric glia of the gastrointestinal tract have a different cell lineage than brain astrocytes; however, they do express *Gfap* (21), thus it was important to determine if the G-SB2KO mice had an absorption defect in the gut causing a reduction in body weight. Glucose absorption as determined by oral glucose tolerance tests was the same between control and G-SB2KO mice (Fig. S6*B*), as were intraperitoneal glucose tolerance tests (Fig. S6*C*). Fecal calorie content, assessed by bomb calorimetry, also showed no evidence of malabsorption in KO mice (Table S1), and there was no evidence of glucose in the urine of any of the mice.

Respiratory Exchange Ratio Is Dramatically Increased in G-SB2KO Mice. To further assess metabolic differences created by the loss of SREBP2 in astrocytes, 4-mo-old female G-SB2KO mice were subjected to metabolic cage assessment. Although food intake over 72 h was equivalent in G-SB2KO and controls (9.98 ± 0.78 vs. 9.30 ± 0.76 g, $P = 0.56$) (Fig. S7*A*), the G-SB2KO mice were less active during the light phase (40 ± 13 vs. 196 ± 35 beam breaks per 15 min, $P < 0.01$) (Fig. 4*C*). This resulted in a decrease in VO_2 during the same period (3,874 ± 88 vs. 4,406 ± 224 mL·h·kg^{-1} lean body weight, $P = 0.05$) (Fig. 4*D*). There was no difference in activity or VO_2 during the dark phase. The most striking difference in the metabolic cage assessment, however, was a dramatic increase in the respiratory exchange ratio (RER) in the G-SB2KO mice during the dark (feeding) phase of the study, (0.92 ± 0.02 vs. 0.81 ± 0.02, $P < 0.001$) (Fig. 4 *E* and *F*). This occurred with no difference in RER between groups in the light phase, when mice are generally sleeping (0.79 ± 0.01 vs. 0.78 ± 0.01, $P = 0.21$). This shift in substrate oxidation toward carbohydrates in fed G-SB2KO mice was observed in younger female mice and was confirmed in 9-mo-old male mice as well (Fig. S7*B*). These results were mirrored by serum-free fatty acids, which were similar in the fasted state between groups, but significantly lower in KO mice after refeeding (Table S1). Of note, refeeding did not increase markers of liver lipogenesis, a potential cause of increased RER (Fig. S7*C*). The lower free-fatty acids were consistent with the reduced size of the fat pads and liver of G-SB2KO mice. The differences in RER were weight-independent, as evidenced by a similar difference in RER between weight-matched control and G-SB2KO mice (Fig. S7 *D* and *E*).

To determine if G-SB2KO mice could properly use a lipid-rich diet, 6-wk-old male G-SB2KO and controls were placed on a high-fat diet. After 7 wk, the G-SB2KO mice only gained 7 g of weight compared with nearly 15 g in the controls (Fig. S8*A*) ($P < 0.01$ for weeks 0–6, $P = 0.02$ for week 7). Metabolic cage assessment of high-fat–fed G-SB2KO mice again showed an increase in RER in the dark phase compared with controls (Fig. S8*B*), although there was less of a difference on normal chow. Thus, despite their preference to use carbohydrate, G-SB2KO mice retain enough metabolic flexibility to metabolize a primarily fat-based diet.

Glucose Oxidation in G-SB2KO Tissues. To more fully define glucose metabolism, G-SB2KO mice and their controls were subjected to hyperinsulinemic clamp studies with [U-^{13}C]–labeled glucose infusion. To better mimic the postprandial state, the clamp was performed at very mild hyperglycemia with blood glucoses of ~135 mg/dL (Fig. S9*A*). These glucose levels were obtained with similar glucose infusion rates [60.1 ± 4.8 for G-SB2KO vs. 67.4 ± 9.4 mg/(kg-min) for controls, $P = 0.45$] (Fig. S9*B*). Under these conditions there was also similar whole-body glucose uptake [64.6 ± 3.6 vs. 71.0 ± 9.0 mg/(kg-min), $P = 0.44$] (Fig. S9*C*), suppression of endogenous glucose production (72.6 ± 14.5 vs. 76.6 ± 16.9%, $P = 0.87$) (Fig. S9*D*), and suppression of nonesterified fatty acids (63.0 ± 7.1 vs. 69.7 ± 9.0%, $P = 0.60$) (Fig. S9*E*) in the G-SB2KO and control mice.

To identify the key tissues involved in the differential flux of carbohydrates, at the end of the clamp individual tissues were dissected, and the ratio of $^{13}C_2$ acetyl CoA to $^{13}C_3$ alanine determined. Under these conditions, the ratio of $^{13}C_2$ acetyl CoA to $^{13}C_3$ alanine provides an assessment of the ratio of flux through pyruvate dehydrogenase (PDH) relative to flux through citrate synthase (CS). These ratios were converted to percentages, with 100% indicating that only oxidized glucose was used in the tricarboxylic acid cycle, and reductions from 100% indicating the relative contribution from fat oxidation and amino acid deamination. As expected, in controls the highest carbohydrate flux was in the brain, with 91.4 ± 1.0% of the labeled glucose in $^{13}C_2$

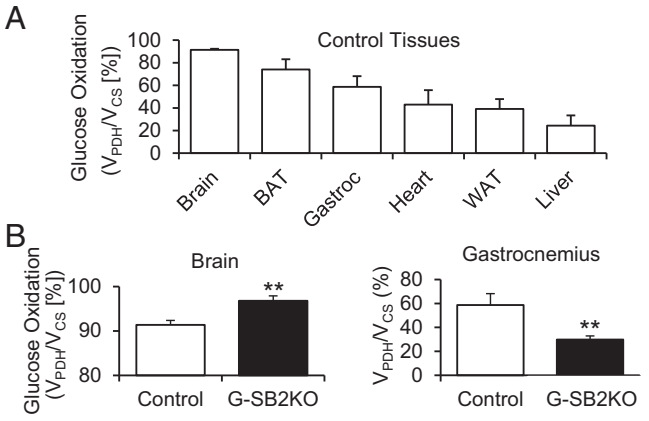

Fig. 5. Glucose oxidation is increased in G-SB2KO brain. A hyperinsulinemic-glucose clamp was performed on 3-mo-old mice, with blood glucose clamped between 120 and 140 mg/dL. Blood glucose was maintained with variable infusion of [U-^{13}C]glucose for 140 min. At the end of the clamp mice were killed and glucose oxidation, expressed as a ratio of flux through PDH to CS (V_{PDH}/V_{CS} %), was determined as described in *Methods* for (*A*) control tissues. (*B*) Differences in V_{PDH}/V_{CS} % for brain and gastrocnemius between control ($n = 5$) and G-SB2KO ($n = 11$). Student's t test $^{**}P < 0.01$.

acetyl CoA, and other tissues showing lower rates (Fig. 5*A*). In the G-SB2KO mice, brain glucose oxidation increased even further to 96.8 ± 1.1% ($P < 0.01$), whereas this ratio decreased in gastrocnemius muscle from 58.6 ± 9.5% in controls to 29.8 ± 3.1 in G-SB2KO mice ($P < 0.01$), with no significant changes in ratio in heart, liver, white or brown fat (Fig. 5*B* and Fig. S9*F*). These data, together with the RER data, suggest that the increased whole-body carbohydrate metabolism in G-SB2KO mice is being driven by brain glucose oxidation at the expense of the muscle.

Discussion

Cholesterol is an integral part of all cell membranes, including neurons and astrocytes. In agreement with studies using retinal ganglion cells (11), we show that in culture glial-conditioned media can support neurite outgrowth and that this is lost by knockdown of SREBP2 in the glia cells, indicating glial cholesterol production as an important contributor to this phenomenon.

To specifically reduce cholesterol synthesis in astroglial cells in vivo, we used Cre-lox technology to inactivate the master transcriptional regulator of the cholesterol synthetic genes, SREBP2, in astrocytes (G-SB2KO). Although the mice are fully viable, the brains of homozygous G-SB2KO mice, which still contain abundant astrocytes, are reduced in size by about 30%, with the greatest reductions in regions rich in astrocytes. Cholesterol content per gram tissue, however, shows only a modest reduction because of increased SREBP2 expression in neurons compensating for the loss in astrocytes.

Despite the partial rescue, G-SB2KO mice exhibit a broad array of behavioral changes. These mice also have a surprising reduction of body mass and are protected from age- and high-fat diet-induced obesity. SREBP2 KO in astrocytes also results in a major increase in RER in the fed state, indicating a shift toward carbohydrate metabolism driven by an increase in brain glucose oxidation.

Although some astrocytes do not express *Gfap* unless activated by an insult, and some adult neural progenitor cells also express *Gfap* (22), this transgene has been shown to be highly expressed in most astrocytes and active as early as E14.5 of gestation (16). It is possible that this results in some elements of progression, because *Gfap*$^-$ astrocytes could become *Gfap*$^+$ with aging, or late neurogenesis could produce neurons with a *Srebp2* KO. Nonetheless, most defects were already present by 3 mo of age and were stable until at least 10 mo of age.

The impact of SREBP2 loss from astrocytes on brain function is evident by multiple measures, including social behavior, learning and memory, and motor coordination. This broad set of behavioral defects is in line with the idea that loss of cholesterol production by astrocytes results in a generalized reduction in the quality and quantity of neuronal synapses. As a result, areas of the brain that have a lower density of astrocytes may be less vulnerable to the disruption in astrocyte cholesterol synthesis.

The alterations in metabolism because of loss of SREBP2 in astrocytes, especially the increase in RER in the fed state, are quite profound. This finding cannot be attributed to an increase in activity or increased sympathetic nervous system activity. Instead, it appears to be because of increased carbohydrate use by the brain, which is already a near obligate user of carbohydrates for fuel. This result became clear when we assessed the relative ^{13}C labeling of $^{13}C_2$ acetyl CoA vs. $^{13}C_3$ alanine as measures of PDH flux relative to CS flux in brain and other tissues. A similar increase in RER during the first half of the dark cycle is observed in mice in which brain cholesterol synthesis was disrupted by heterozygous KO of SCAP (8). In the latter, in which regulation of cholesterol synthesis is disrupted in both neurons and glia, there is also an increase in VO_2 and activity, suggesting additional mechanisms may be involved.

G-SB2KO mice also show an inability to accumulate fat on either a normal diet or high-fat diet. The difference in body weight and fat accumulation between control and G-SB2KO mice is not accounted for by an increase in energy expenditure or by caloric loss in urine or stool. Rather, the reduction in carbohydrate oxidation in muscle, and trends toward reductions in fat and liver, suggest that calories that might normally go to protein synthesis or lipogenesis are being diverted away to the brain, resulting in the smaller tissue weights of these other organs. The reason for the increased requirement for glucose by the brain is not clear; however, it may be that, in the absence of astrocyte-derived cholesterol, neurons become more active, consuming additional energy, or synthesize cholesterol less efficiently than astrocytes. Additionally, astrocytes are able to use a wider range of fuels than neurons, such as acetate (23). If neurons are forced to produce additional cholesterol, it would be expected that this might result in additional glucose consumption.

There is a strong link between diabetes, insulin resistance in the brain, and AD (24–27). Loss of insulin action in the brain also causes increased phosphorylation of tau protein, an early marker of AD (26). Amyloid-β, another marker of AD pathology, is cleared from the brain by insulin degrading enzyme, and it has been proposed that increased insulin in the brain, particularly in type 2 diabetes, results in competition for this enzyme, allowing for an increased build-up of amyloid-β around neurons (reviewed in ref. 28). Although these may be contributors to the link between diabetes and AD, it is clear that tau phosphorylation itself is not enough to trigger AD and that plaque quantity is not a perfect predictor of disease severity (29, 30). Preliminary clinical trials using intranasal insulin in patients with AD, but not diabetes, have shown some effectiveness on dementia symptoms (31), arguing that lack of insulin or insulin activity, rather than surplus insulin, may be a contributor to diabetes-associated AD. Subgroup analysis suggests that ApoE ε4 carrier status increases the response to intranasal insulin, implying an insulin–cholesterol relationship in this patient population (32). Furthermore, we and others have shown that knockdown or inhibition of cholesterol synthesis from neurons creates insulin resistance in those cells (33, 34), suggesting a feed-forward connection between diabetes and AD.

There is epidemiological evidence that increased serum cholesterol is associated with AD (14); however, cholesterol does not significantly cross the blood–brain barrier, and large randomized controlled clinical trials using cholesterol-lowering statin drugs showed little impact on AD progression (14). Although there are many possibilities for the failure of these trials, including low penetration of the drugs into the brain, our data suggest that lowering brain cholesterol levels could actually have a detrimental effect on brain function. In fact, sporadic reports of short-term memory loss associated with statin therapy have

prompted the Food and Drug Administration to put a warning on the drug class (35). Furthermore, hyperlipidemia is often associated with insulin resistance as part of the metabolic syndrome. It may be that systemic insulin resistance is either causing reduced insulin transport into the brain (36) or impaired insulin signaling within the brain (25), which in turn could be causing a reduction in cholesterol synthesis. Further studies need to be directed at measuring brain insulin resistance and brain cholesterol levels in humans to help understand the roles of these pathways in the interaction between diabetes and altered brain function.

Methods

Lentiviral Silencing of SREBP2 in Glioma Cells. C6 rat glioma cells were stably infected with lentiviral vector plasmids for *Srebf2* shRNA or control scrambled shRNA.

Neurite Outgrowth. GT1-7 cells were grown in 15.6-mm wells with transwells containing C6 shSrebf2 or C6 shScramble cells. Neurite length was measured using the NeuronJ plugin for ImageJ.

Animals. *Srebf2*$^{lox/lox}$ mice were created using a targeting construct with lox sites flanking exon 1 and a neomycin selection cassette. These mice were crossed to GFAP-Cre mice expressing a 2.2-kb fragment of the human GFAP promoter (16). All animal studies followed the National Institutes of Health guidelines and were approved by the Institutional Animal Care and Use Committees at the Joslin Diabetes Center or the Yale University School of Medicine.

Histology. Frozen sections of brain were stained using antibodies against GFAP (MAB360, EMD Millipore) and SREBP2 (LS-B1609, Lifespan Biosciences).

Behavioral Testing. Nest building, Stone T-maze, and balance beam were performed to assess social, learning and memory, and motor function, respectively, as described in detail in *SI Methods*.

Body Composition and Metabolic Testing. Metabolic cage testing was performed using a Comprehensive Laboratory Animal Monitoring System (CLAMS; Columbus Instruments).

V_{PDH}/V_{CS} Measurement. Hyperinsulinemic-glucose clamps were performed in awake mice as previously described (37). At the end of the clamp, relative flux through PDH (V_{PDH}) and CS (V_{CS}) pathways in individual tissues was assessed as the ratio of $^{13}C_2$ acetyl CoA to $^{13}C_3$ alanine (i.e., the precursor and product of PDH flux). To measure tissue acetyl CoA content, ~50 mg of tissue was homogenized in 1 mL of 10% (vol/vol) trichloroacetic acid. The extraction and LC/MS/MS were performed with atom percent enrichments calculated as described previously (38). Total alanine enrichment was measured by GC/MS.

ACKNOWLEDGMENTS. We thank Megan Krumpoch and Noelle Castilla-Ojo for animal care. These studies were funded by National Institute of Diabetes, Digestive and Kidney Diseases Grants 5K08DK097293 (to H.A.F.), R01 DK-40936 and MMPC DK059635 (to G.I.S.), and R37DK031036 (to C.R.K.); and Diabetes Research Center Grants P30DK036836 (to the Joslin Diabetes Center) and P30CA06516 (to the Rodent Histopathology Core at Dana-Farber/Harvard Cancer Center).

1. Pfrieger FW, Ungerer N (2011) Cholesterol metabolism in neurons and astrocytes. *Prog Lipid Res* 50(4):357–371.
2. Brown MS, Goldstein JL (2009) Cholesterol feedback: From Schoenheimer's bottle to Scap's MELADL. *J Lipid Res* 50(Suppl):S15–S27.
3. Dietschy JM, Turley SD (2004) Thematic review series: Brain ipids. cholesterol metabolism in the central nervous system during early development and in the mature animal. *J Lipid Res* 45(8):1375–1397.
4. Balazs Z, et al. (2004) Uptake and transport of high-density lipoprotein (HDL) and HDL-associated alpha-tocopherol by an in vitro blood-brain barrier model. *J Neurochem* 89(4):939–950.
5. Schönfeld P, Reiser G (2013) Why does brain metabolism not favor burning of fatty acids to provide energy? Reflections on disadvantages of the use of free fatty acids as fuel for brain. *J Cereb Blood Flow Metab* 33(10):1493–1499.
6. Miao J, et al. (2014) Hepatic insulin receptor deficiency impairs the SREBP-2 response to feeding and statins. *J Lipid Res* 55(4):659–667.
7. Suzuki R, et al. (2010) Diabetes and insulin in regulation of brain cholesterol metabolism. *Cell Metab* 12(6):567–579.
8. Suzuki R, Ferris HA, Chee MJ, Maratos-Flier E, Kahn CR (2013) Reduction of the cholesterol sensor SCAP in the brains of mice causes impaired synaptic transmission and altered cognitive function. *PLoS Biol* 11(4):e1001532.
9. Fields RD, Woo DH, Basser PJ (2015) Glial regulation of the neuronal connectome through local and long-distant communication. *Neuron* 86(2):374–386.
10. Volterra A, Liaudet N, Savtchouk I (2014) Astrocyte Ca^{2+} signalling: An unexpected complexity. *Nat Rev Neurosci* 15(5):327–335.
11. Mauch DH, et al. (2001) CNS synaptogenesis promoted by glia-derived cholesterol. *Science* 294(5545):1354–1357.
12. Liu Q, et al. (2010) Neuronal LRP1 knockout in adult mice leads to impaired brain lipid metabolism and progressive, age-dependent synapse loss and neurodegeneration. *J Neurosci* 30(50):17068–17078.
13. Barbero-Camps E, Fernández A, Martínez L, Fernández-Checa JC, Colell A (2013) APP/PS1 mice overexpressing SREBP-2 exhibit combined Aβ accumulation and tau pathology underlying Alzheimer's disease. *Hum Mol Genet* 22(17):3460–3476.
14. McGuinness B, et al. (2010) Statins for the treatment of dementia. *Cochrane Database Syst Rev* (8):CD007514.
15. LaDu MJ, et al. (1998) Nascent astrocyte particles differ from lipoproteins in CSF. *J Neurochem* 70(5):2070–2081.
16. Bajenaru ML, et al. (2002) Astrocyte-specific inactivation of the neurofibromatosis 1 gene (NF1) is insufficient for astrocytoma formation. *Mol Cell Biol* 22(14):5100–5113.
17. Camargo N, et al. (2012) High-fat diet ameliorates neurological deficits caused by defective astrocyte lipid metabolism. *FASEB J* 26(10):4302–4315.
18. Morales-Corraliza J, et al. (2013) Immunization targeting a minor plaque constituent clears β-amyloid and rescues behavioral deficits in an Alzheimer's disease mouse model. *Neurobiol Aging* 34(1):137–145.
19. Pistell PJ, Ingram DK (2010) Development of a water-escape motivated version of the Stone T-maze for mice. *Neuroscience* 166(1):61–72.
20. Morrison SF, Madden CJ (2014) Central nervous system regulation of brown adipose tissue. *Compr Physiol* 4(4):1677–1713.
21. Coelho-Aguiar JdeM, et al. (2015) The enteric glia: Identity and functions. *Glia* 63(6):921–935.
22. Sofroniew MV (2012) Transgenic techniques for cell ablation or molecular deletion to investigate functions of astrocytes and other GFAP-expressing cell types. *Methods Mol Biol* 814:531–544.
23. Waniewski RA, Martin DL (1998) Preferential utilization of acetate by astrocytes is attributable to transport. *J Neurosci* 18(14):5225–5233.
24. Kleinridders A, Ferris HA, Cai W, Kahn CR (2014) Insulin action in brain regulates systemic metabolism and brain function. *Diabetes* 63(7):2232–2243.
25. Talbot K, et al. (2012) Demonstrated brain insulin resistance in Alzheimer's disease patients is associated with IGF-1 resistance, IRS-1 dysregulation, and cognitive decline. *J Clin Invest* 122(4):1316–1338.
26. Schubert M, et al. (2004) Role for neuronal insulin resistance in neurodegenerative diseases. *Proc Natl Acad Sci USA* 101(9):3100–3105.
27. Bomfim TR, et al. (2012) An anti-diabetes agent protects the mouse brain from defective insulin signaling caused by Alzheimer's disease- associated Aβ oligomers. *J Clin Invest* 122(4):1339–1353.
28. Yang Y, Song W (2013) Molecular links between Alzheimer's disease and diabetes mellitus. *Neuroscience* 250:140–150.
29. Bennett DA, Schneider JA, Arvanitakis Z, Wilson RS (2012) Overview and findings from the religious orders study. *Curr Alzheimer Res* 9(6):628–645.
30. Bennett DA, et al. (2012) Overview and findings from the rush Memory and Aging Project. *Curr Alzheimer Res* 9(6):646–663.
31. Craft S, et al. (2012) Intranasal insulin therapy for Alzheimer disease and amnestic mild cognitive impairment: A pilot clinical trial. *Arch Neurol* 69(1):29–38.
32. Claxton A, et al. (2013) Sex and ApoE genotype differences in treatment response to two doses of intranasal insulin in adults with mild cognitive impairment or Alzheimer's disease. *J Alzheimers Dis* 35(4):789–797.
33. Fukui K, Ferris HA, Kahn CR (2015) Effect of cholesterol reduction on receptor signaling in neurons. *J Biol Chem* 290(44):26383–26392.
34. Fox TE, et al. (2011) Insulin signaling in retinal neurons is regulated within cholesterol-enriched membrane microdomains. *Am J Physiol Endocrinol Metab* 300(3):E600–E609.
35. FDA (2012) FDA Drug Safety Commision: Important safety label changes to cholesterol-lowering statin drugs. Available at www.fda.gov/drugs/drugsafety/ucm293101.htm. Accessed August 1, 2016.
36. Craft S, et al. (1998) Cerebrospinal fluid and plasma insulin levels in Alzheimer's disease: Relationship to severity of dementia and apolipoprotein E genotype. *Neurology* 50(1):164–168.
37. Camporez JP, et al. (2013) Cellular mechanism by which estradiol protects female ovariectomized mice from high-fat diet-induced hepatic and muscle insulin resistance. *Endocrinology* 154(3):1021–1028.
38. Perry RJ, et al. (2015) Hepatic acetyl CoA links adipose tissue inflammation to hepatic insulin resistance and type 2 diabetes. *Cell* 160(4):745–758.
39. Shimano H, et al. (1996) Overproduction of cholesterol and fatty acids causes massive liver enlargement in transgenic mice expressing truncated SREBP-1a. *J Clin Invest* 98(7):1575–1584.
40. Zhuo L, et al. (1997) Live astrocytes visualized by green fluorescent protein in transgenic mice. *Dev Biol* 187(1):36–42.
41. Carter RJ, Morton J, Dunnett SB (2001) Motor coordination and balance in rodents. *Current Protocols in Neuroscience* 8:8.12.
42. Brooks SP, Dunnett SB (2009) Test to assess motor phenotype in mice: A user's guide. *Nat Rev Neurosci* 10(7):519–529.
43. Petersen KF, et al. (2015) Effect of aging on muscle mitochondrial substrate utilization in humans. *Proc Natl Acad Sci USA* 112(36):11330–11334.